DOI: 10.1021/ma901035e

Macromolecules
ARTICLE

Nonlinear Effects in the Nanophase Segregation of Polyelectrolyte Gels

Prateek K. Jha,[†] Francisco J. Solis,[∥] Juan J. de Pablo,[⊥] and Monica Olvera de la Cruz*[,†,‡,§]

[†]*Department of Chemical and Biological Engineering and* [‡]*Department of Materials Science and Engineering and* [§]*Department of Chemistry, Northwestern University, Evanston, Illinois 60208,* [∥]*Department of Integrated Natural Sciences, Arizona State University, Glendale, Arizona 85306, and* [⊥]*Department of Chemical and Biological Engineering, University of Wisconsin-Madison, Madison, WI 53706*

Received May 12, 2009; Revised Manuscript Received June 23, 2009

ABSTRACT: Polyelectrolyte gels with hydrophobic backbones exhibit complex phase behavior, such as the formation of various nanophases, that involves local segregation of the monomers. The formation of these inhomogeneous phases is mainly the consequence of the possible interactions on different length scales in the system, with electrostatic effects dominating over large length scales. In this work, we demonstrate the formation of nanophases in a model for a system of salt-free gel that incorporates entropic, elastic, electrostatic as well as solvent interactions. In particular, we analyze the system using both linear and nonlinear methods. Whereas the linear approximation properly identifies the region of instability against nanophase formation, it does not properly describe such nonlinear effects as the formation of very sharp interfaces between the nanosegregated regions. We further investigate the periodicity dependence as well as monomer and charge distributions for the gel as functions of different physical system parameters. Consequently, we determine that the range of solvent quality for nanophase segregation increases with increasing charge fraction and decreasing cross-link density.

Introduction

Polyelectrolyte (PE) gels are increasingly being used for a variety of applications that include superabsorbers, drug delivery devices, artificial muscles, and actuators in microfluidics.[1−7] The 3D network structure, along with a fine interplay of competing elastic, entropic, electrostatic as well as van der Waals interactions, endows them with a very rich phase behavior. For networks in good solvents, the effects of the van der Waals and electrostatic forces between monomers are both repulsive, which leads to general swelling to the extent as permitted by the elasticity of the network. However, these two types of interactions between monomers compete with each other in poor solvents, resulting in the formation of finite-size domains or nanostructures.[8] The presence of cross-links in PE gels further constrains the size of the consequent domains and reduces the possibility of macrophase separation. In recent experiments,[9] the formation of nanosized domains, with sizes on the order of the wavelength of the concentration inhomogeneities, has been observed. In particular, large volume changes in charged gels have been found to be associated with a nanophase or microphase segregation transition. Moreover, the domain sizes can be further controlled by the addition of salts, which would screen the underlying electrostatic interactions and lead to a corresponding increase in entropic forces, as well as by varying such environmental conditions as the solution pH, temperature, or electric field.

Unlike the well studied swelling−deswelling phenomenon of polymer gels, a complete understanding of the formation of nanophases and the corresponding nanopatterns is still lacking because of the theoretical difficulties in dealing with the static (frozen) inhomogeneities and the dynamic (thermal) fluctuations[8] therein. Prior theoretical approaches[10−12] have not accounted for the nonlinear effects in the free energy. As such, the explication and classification of nanodomains remains a challenging problem. In this work, we propose a model of salt-free PE gels with 1D inhomogeneities that explicitly take into account electrostatic fluctuations. Furthermore, a numerical minimization of the resulting free-energy functional establishes the conditions that lead to the formation of nanophases. In particular, we show here that the nonlinear treatment predicts considerable deviations from the conventional random phase approximation (RPA) technique. Because we consider a 1D model, the results are directly applicable to only lamellar nanostructures, although our results may provide guidance for the investigation of other structures.

*Corresponding author. E-mail: m-olvera@northwestern.edu.

Model

We assume that the gel is prepared by cross-linking linear, cationic PE chains under θ-solvent conditions and thus has a Gaussian chain distribution at preparation. We further assume the network to be regular and monodisperse, which enables us to approximate the gel as a periodic array of cubes that form between the cross-links. In the absence of inhomogeneities, this model gel will always isotropically deform to a new state that minimizes the free energy for given physical conditions (e.g., solvent quality, charge fraction, cross-link density, etc.). However, the presence of inhomogeneities might favor a phase-separated state if they are not suppressed by the competing interactions. Because we consider inhomogeneities to be present in one direction, a lamellar phase can be attained in the microphase-separation regime.

The phase behavior of our model gel can be visualized by the representation in Figure 1a, where we assume the inhomogeneities to be present in the x direction. In the event of phase separation, we expect a lamellar phase with alternating dense and depleted regions. The periodicity (λ) of this lamellar phase, in turn, characterizes the regime of phase separation. A finite value of λ indicates the microphase-separated gel, wherein the numerical values of λ in the nanometer range indicate the existence of nanophases. In particular, macrophase separation is attained when $\lambda \to \infty$, and $\lambda = 0$ corresponds to the homogeneous (isotropic)

 Published on Web 07/10/2009

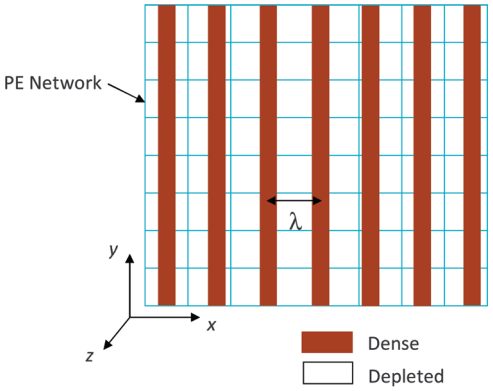

(a)

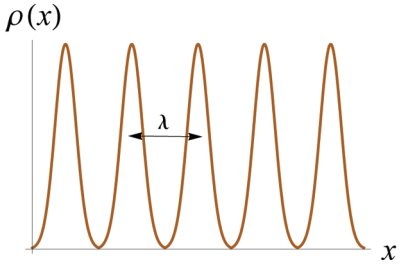

(b)

Figure 1. (a) Schematic showing the phase behavior of phase-separated gel for inhomogeneities along the x direction. (b) Typical excess charge density profile in the micro(nano)phase-separated gel.

phase. The dense and depleted regions in Figure 1a correspond to the polymer- and solvent-rich phases, respectively. This classification of these two phases can be more precisely quantified by the introduction of the excess charge density defined as $\rho(x) = s(x) - f\phi(x)$, where $s(x)$ and $\phi(x)$ are the local counterion and the polymer volume fractions, respectively. The quantity f represents the fraction of charged monomers. Figure 1b shows the typical excess charge density profile in the microphase-separated regime. Note that the volume fractions $[\phi(x),s(x)]$ are local, and the inhomogeneity is assumed to occur on a smaller length scale than the distance between the cross-links. This assumption is necessary because it has been shown that microphase-segregated nanogels with dimensions of the order of the density fluctuations L^* do not undergo nanophase segregation.[9] Moreover, after the gel reaches a critical size, the resulting patterns have been found to be size-independent. In our model, the PE gel is assumed to be sufficiently larger than its critical size so that we can neglect the boundary effects in the free energy. We then compute the free energy for an infinitesimal volume $\Delta V = A\Delta x$, where A is the area in the direction perpendicular to the direction of inhomogeneities and Δx is an infinitesimal length in the x direction. The polymer and counterion volume fractions are both assumed to be constant in this infinitesimal volume. The free energy per unit volume for the entire gel is then obtained by integrating this free energy over the region $0 \le x \le \lambda$, followed by division by the volume of the region $A\lambda$.

The free energy of the PE gel contains both solvent entropic and mixing contributions that are evaluated in the mean-field limit using the Flory−Huggins model

$$\frac{\Delta F_{\mathrm{solv}} a^3}{k_{\mathrm{B}} T \Delta V} = \chi\phi(1-\phi) + (1-\phi)\ln(1-\phi) \tag{1}$$

Here the quantity χ characterizes the solvent quality, with T and k_{B} representing the temperature and the Boltzmann constant, respectively. In the above and subsequent equations, local volume fractions $[\phi(x),s(x)]$ are written as $[\phi,s]$ for brevity. Inhomogeneities modify the elastic free energy, and the resulting expression can be derived by constructing a locally varying deformation tensor.[11] However, this approach assumes Gaussian chain distribution for polymer chains between the cross-links and is not valid for highly compressed/stretched chains. Therefore, we use another approach whereby the mean extension of a single polymer chain ($\langle h(\mathscr{F})\rangle$) is related to the net stretching force ($\mathscr{F}$) via the Langevin function $L(\mathscr{F})$, that is

$$H = \frac{\langle h(\mathscr{F})\rangle}{h_{\max}} = L(\mathscr{F}) = \coth(\mathscr{F}) - \frac{1}{\mathscr{F}} \tag{2}$$

Here the quantity $h_{\max} = Na$ is the maximum chain extension, where N is the number of monomers between cross-links and a is the monomer size. The quantity H is a dimensionless variable representing the scaled chain extension. The Langevin function forbids the stretching of the chain to length values higher than the maximum possible stretching ($\mathscr{F} \to \infty$ when $H \to 1$). Because the Langevin function cannot be inverted analytically, we use the interpolation formula for the stretching force in the range $0 < H < 1$, obtained by inverting the series expansions of Langevin function in the limits of $H \ll 1$ and $1 - H \ll 1$[13]

$$\mathscr{F}(H) = \frac{3H - H^3}{1 - H^2} \tag{3}$$

In eq 3, the quantity H can be related to the volume fractions in the actual state and to the hypothetical state in which all chains are stretched to the maximum possible extension. Volume fraction in that hypothetical state is given by $\phi_{\max} = 3Na^3/(Na)^3 = 3/N^2$. Therefore, for the homogeneously deformed gel

$$H = \frac{\langle h(\mathscr{F})\rangle}{h_{\max}} = \left(\frac{\phi_{\max}}{\bar{\phi}}\right)^{1/3} = \left(\frac{3}{N^2\bar{\phi}}\right)^{1/3} \tag{4}$$

where $\bar{\phi}$ is the volume fraction of the isotropically deformed state. To account for the presence of inhomogeneities, we define local scaled extensions as

$$H(x) = \sqrt{\frac{2}{3}\left(\frac{\phi_{\max}}{\bar{\phi}}\right)^{2/3} + \frac{1}{3}\left(\frac{\phi_{\max}}{\phi}\right)^{2/3}} = \sqrt{\zeta\left(1 + \frac{\bar{\phi}^2}{2\phi^2}\right)} \tag{5}$$

where we have used the fact that the extension in two directions is the same as the homogeneously deformed case, and $\zeta = 2/(3^{1/3}N^{4/3}\bar{\phi}^{2/3})$. Note that we can uniquely define an isotropically deformed state with volume fraction ϕ for all states of the gel that correspond to a given cross-link density or a given gel volume. In what follows, we take it as a fixed parameter only to determine the nanostructure with respect to an isotropically swollen state as a reference state.

The elastic free energy is then evaluated by integrating $\mathscr{F}(H)$ with respect to H. Upon simplifying, our elastic free energy in dimensionless form follows

$$\frac{\Delta F_{\mathrm{elas}} a^3}{k_{\mathrm{B}} T \Delta V} = \zeta\left(\phi + \frac{\bar{\phi}^2}{2\phi}\right)/6 - \frac{\phi}{3}\ln\left[1 - \zeta\left(1 + \frac{\bar{\phi}^2}{2\phi^2}\right)\right] \tag{6}$$

The effect of inhomogeneities is included by an additional

concentration gradient term in the free energy[11]

$$\frac{\Delta F_{\mathrm{gra}}}{k_{\mathrm{B}}T\Delta V} = \frac{C}{2}|\nabla\phi|^2 \tag{7}$$

The parameter $C \approx k_{\mathrm{B}}T/(a\bar{\phi})$ is positive, as predicted by scaling theory for polymers in θ solvents.[14] The use of RPA for polymer solutions[11] leads to similar scaling, but the values of C can vary by corresponding factors in the high-q ($\sim k_{\mathrm{B}}T/[12a\bar{\phi}(1-\bar{\phi})]$) and low-$q$ ($\sim k_{\mathrm{B}}T/[18a\bar{\phi}(1-\bar{\phi})]$) limits. Because we are only interested in the behavior at finite periodicity, we choose the RPA value in the low-q limit throughout our analysis. Note that the use of the gradient term to explain the effects of inhomogeneities is a standard practice in condensed-matter physics[15] and can be thought of as interfacial forces that result from concentration gradients in the system.

The effect of charge enters into the free energy in two ways: through the translational entropy of counterions as follows

$$\Delta F_{\mathrm{ion}}a^3/(k_{\mathrm{B}}T\Delta V) = s\ln s \tag{8}$$

and in the Coulombic interaction energy as given by[16]

$$F_{\mathrm{elec}} = \frac{A^2}{8\pi\varepsilon}\int\int\frac{\rho(x)\rho(x')}{|x-x'|}\,\mathrm{d}x\,\mathrm{d}x' = \frac{A}{2}\int\rho(x)\Phi(x)\,\mathrm{d}x \tag{9}$$

Here the quantity ε denotes the dielectric constant of the solvent, and $\Phi(x)$ is the electrostatic potential at location x. Note that the Coulombic energy is not present in the isotropically deformed case because there is no excess charge in the system as a result of electroneutrality. In our present model, global electroneutrality is satisfied but allowed to be violated locally because of the presence of inhomogeneities. In turn, this gives rise to the Coulombic interaction term that is otherwise absent in the isotropically deformed case. As usual, the electrostatic potential is related to the charge density via the Poisson equation, $\nabla^2\Phi = -\rho/\varepsilon$. To simplify the evaluation of the electrostatic energy, we use the Green's function approach,[17] where the Green's function also has the same periodicity (λ) as the ion densities. The required Green's function is determined by imposing the periodic boundary conditions, $G(0) = G(\lambda)$ and $(\mathrm{d}G/\mathrm{d}x)|_{x=0} = (\mathrm{d}G/\mathrm{d}x)|_{x=\lambda}$, on its defining equation

$$\frac{\mathrm{d}^2G(x-x')}{\mathrm{d}x^2} = -4\pi\delta(x-x') + \frac{4\pi}{\lambda};\quad 0 < x-x' < \lambda \tag{10}$$

which physically describes a point source with a uniform background consisting of the opposite charge. Therefore, the electrostatic potential at a location x can be written as

$$\Phi(x) = \frac{A}{4\pi\varepsilon}\int_0^\lambda\rho(x')G(x-x')\,\mathrm{d}x' \tag{11}$$

Combining eqs 9 and 11, we obtain an alternative expression for the Coulombic interaction as follows

$$\frac{F_{\mathrm{elec}}a^3}{k_{\mathrm{B}}TV} = \frac{l_{\mathrm{B}}}{2\lambda}\int_0^\lambda\int_0^\lambda\rho(x)G(x-x')\rho(x')\,\mathrm{d}x'\,\mathrm{d}x \tag{12}$$

Here the quantity $l_{\mathrm{B}} = e^2/(4a\pi\varepsilon k_{\mathrm{B}}T)$ is the dimensionless Bjerrum length [typically of $O(1)$]. Consequently, the 1D Green's function that satisfies both eq 10 and the periodic boundary conditions is given by

$$G(x-x') = \frac{2\pi}{\lambda}[(x-x')^2 - \lambda|x-x'|] \tag{13}$$

The total free energy per unit volume of the gel can now be written as the sum of eq 12 and a mean field term derived from eqs 1, 6, 7, and 8

$$\frac{F_{\mathrm{mean}}a^3}{k_{\mathrm{B}}TV} = \frac{1}{\lambda}\int_0^\lambda\left[\zeta\left(\phi+\frac{\bar{\phi}^2}{2\phi}\right)/6 - \frac{\phi}{3}\ln\left\{1-\zeta\left(1+\frac{\bar{\phi}^2}{2\phi^2}\right)\right\}\right.$$
$$\left.+\chi\phi(1-\phi) + (1-\phi)\ln(1-\phi) + s\ln s + C\left(\frac{\partial\phi}{\partial x}\right)^2\right]\mathrm{d}x \tag{14}$$

Equations 12 and 14 are being made dimensionless by scaling all lengths by the monomer size a. In the subsequent discussion, the length variables are presumed to be dimensionless. Because the isotropically deformed gel has the same overall volume as the anisotropic gel, we also need to satisfy the balance constraints

$$\int_0^\lambda[\phi(x)-\bar{\phi}]\,\mathrm{d}x = 0;\quad \int_0^\lambda[s(x)-\bar{s}]\,\mathrm{d}x = 0 \tag{15}$$

Imposing these constraints, we automatically satisfy the global electroneutrality condition

$$\int_0^\lambda[s(x)-f\phi(x)]\,\mathrm{d}x = 0 \tag{16}$$

Minimization of the free energy functional given by the sum of eqs 12 and 14, subject to the balance constraints (eq 15), yields the density profiles and the periodicity of the system. To minimize the free energy functional, we develop a finite difference-based scheme where we fix the value of λ and discretize the domain $0 \le x < \lambda$ into M elements. The above integrals are then reduced to sums, and we are left with a univariate-constrained minimization problem with variables ϕ_i and s_i ($i = 1, 2, ..., M$) representing the volume fractions of polymer and counterions at M evenly spaced locations in the interval of $0 \le x \le \lambda$. Numerical minimization is performed using the gradient-projection algorithm[18,19] to evaluate the density profiles that minimize the free energy for a given fixed λ. Repeating this process for different values of λ yields the optimal periodicity and density profiles.

To estimate the range of the model parameters for nanophase formation, we use RPA to obtain an instability matrix in the domain frequency via harmonic perturbations of the order parameters $[\phi(x),s(x)]$ to the second order. The Hessian matrix is given by

$$A = \begin{bmatrix} \dfrac{\delta^2\hat{F}}{\delta\bar{\phi}^2} & \dfrac{\delta^2\hat{F}}{\delta\bar{\phi}\delta\bar{s}} \\ \dfrac{\delta^2\hat{F}}{\delta\bar{\phi}\delta\bar{s}} & \dfrac{\delta^2\hat{F}}{\delta\bar{s}^2} \end{bmatrix}$$
$$= \begin{bmatrix} \dfrac{\zeta\{12+\zeta(-16+9\zeta)\}}{6(2-3\zeta)^2\bar{\phi}} - 2\chi + \dfrac{1}{1-\bar{\phi}} + \dfrac{l_{\mathrm{B}}f^2}{k^2} + Ck^2 & \dfrac{-l_{\mathrm{B}}f}{k^2} \\ \dfrac{-l_{\mathrm{B}}f}{k^2} & \dfrac{1}{f\bar{\phi}} + \dfrac{l_{\mathrm{B}}}{k^2} \end{bmatrix} \tag{17}$$

where $\hat{F} = Fa^3/(k_{\mathrm{B}}TV)$ and k ($= 2\pi/\lambda$) is the dominant wavevector of the perturbations. Note that the first-order terms are canceled by symmetry. The eigenvalues of the matrix **A** quantify the stability of the system against inhomogeneities. The matrix **A** is a 2×2 symmetric matrix with real elements for our system parameters of interest and can be shown also to have real eigenvalues. We denote the maximum and minimum eigenvalues by $\lambda_+(k)$ and $\lambda_-(k)$, respectively. Spinodals for regimes of microphase and macrophase separation are then defined by the

conditions $\{\lambda_{-}(k^*) = 0$ and $(d\lambda_{-}(k)/dk)|_{k^*} = 0$ for a finite $k^* > 0\}$ and $\{\lambda_{-}(0) = 0$ and $(d\lambda_{-}(k)/dk)|_{k=0} = 0\}$, respectively.[10] The spinodal lines can be expressed in terms of critical solvent qualities χ_{mi} (microphase) and χ_{ma} (macrophase) as

$$\chi_{mi} = \frac{1}{2}\left[2f\sqrt{Cl_B} - Cl_B f\overline{\phi} + \frac{1}{1-\overline{\phi}} + \frac{\zeta\{12+\zeta(-16+9\zeta)\}}{6(2-3\zeta)^2\overline{\phi}}\right]$$

$$\chi_{ma} = \frac{1}{2}\left[\frac{f}{\overline{\phi}} + \frac{1}{1-\overline{\phi}} + \frac{\zeta\{12+\zeta(-16+9\zeta)\}}{6(2-3\zeta)^2\overline{\phi}}\right] \quad (18)$$

Therefore, in the RPA treatment, the system is expected to be isotropic for $\chi < \chi_{mi}$, microphase-separate for $\chi_{mi} < \chi < \chi_{ma}$, and macrophase-separate for $\chi > \chi_{ma}$. The optimal periodicity in this approach is λ^* $(= 2\pi/k^*)$, which leads to the largest negative eigenvalue in the microphase regime.

Results and Discussion

Our choice of the model parameters is governed by the objective of capturing all possible phases in the model gel. RPA analysis provides initial estimates of the critical values of the model parameters for microphase/macrophase segregation as well as of the optimal periodicity. Numerical minimization is then carried for a range of parameters close to these seed values, which proves to be a good choice in that the linear theory correctly identifies the regions of instability. In particular, Figure 2 shows the results of our numerical minimization. At low values of χ ($\chi \leq 2.4$ in Figure 2), the free energy remains constant with periodicity and implies no phase separation. For intermediate values of χ ($2.4 \leq \chi \leq 3.5$ in Figure 2), a clear minimum exists at a given finite periodicity, thereby signaling microphase separation. The optimal periodicity is 5−10 times the monomer size, which thus confirms the existence of nanosized domains (nanophases). Upon further increasing χ while keeping other parameters constant, the free energy passes through an inflection point to become a monotonically decreasing function with a minimum at $\lambda \rightarrow \infty$ signaling macrophase separation. Figure 3 illustrates the excess charge density, monomer density, and counterion density profiles at the optimal periodicity in the nanophase regime. Profiles for the lowest χ value in these plots indicate an isotropic phase where the densities are essentially constant. For other values of χ, we observe the formation of a dense region of monomers, followed by a depleted region, as is expected for a lamellar structure. The dense region in the polymer/excess charge−density profile gets sharper with increasing χ until it reaches the macrophase regime. Whereas the interfacial energy (described by the gradient term in eq 7) and the Coulombic interaction drive the polymer chains toward the formation of sharp profiles, the entropic forces are the dominant interaction for the counterions that result in weak segregation.

Next, we compare the results of the nonlinear theory with those of the linear theory based on RPA. Figure 4 shows the optimal periodicity that has been evaluated using the two approaches for a range of values of χ and N. Whereas the optimal λ evaluated from the linear theory is almost constant (slight downhill slope), the nonlinear theory shows phase-transition-like behavior. Moreover, the values of optimal λ in the nonlinear theory are found to be lower than those in the linear theory. Figure 5a,b shows the plots of critical solvent qualities (χ_{mi} and χ_{ma}, as defined by eq 18 for the RPA and numerically evaluated in the nonlinear approach) as functions of f and ϕ, respectively. We observe that the range of solvent quality for nanophase separation takes on larger values for higher charge fraction of monomers (Figure 5a) and lower cross-link density (or lower equilibrium volume

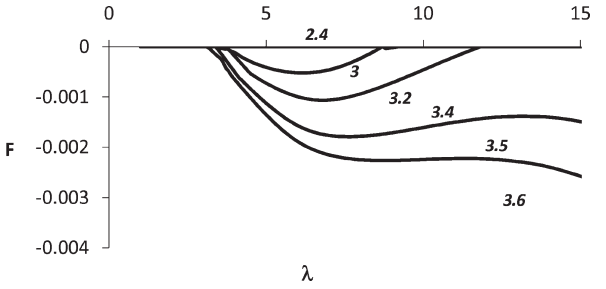

Figure 2. Free energy minimum against periodicity for a range of solvent quality (χ). Free energy is defined as the difference between that of the actual state and the isotropically deformed state of gel. The model parameters are $\phi = 0.05$, $l_B = 1$, $N = 100$, and $f = 0.5$.

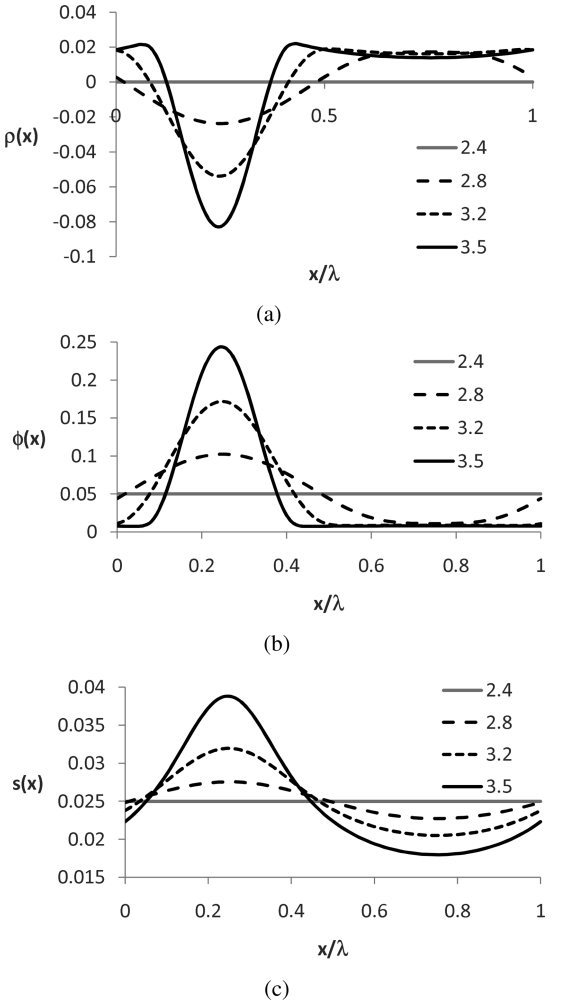

Figure 3. Profiles of (a) excess charge density, (b) monomer density, and (c) counterion density for a range of solvent quality. Densities are reported in terms of volume fractions. The model parameters are $\phi = 0.05$, $l_B = 1$, $N = 100$, and $f = 0.5$.

fraction $\overline{\phi}$ as shown in Figure 5b). As evident from these plots, the region of micro(nano)phase separation (between the dashed lines) is significantly reduced when compared with the RPA predictions (between the bold lines). The discrepancy can be attributed to the improper treatment of the energy of electrostatic fluctuations and the interfacial energy expression found in the RPA approach. More specifically, the nonlinear terms become significant at the instance a nanophase is formed.

The transition between an isotropic state with weak density inhomogeneities and a strongly correlated periodic nanophase is

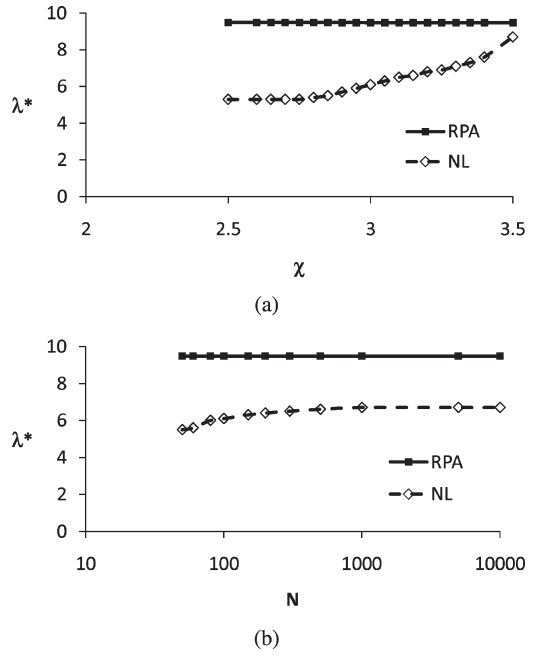

Figure 4. Optimal periodicity against (a) solvent quality and (b) number of monomers between cross-links evaluated by the RPA and by the nonlinear (NL) analysis. The model parameters are $\bar{\phi} = 0.05$, $l_B = 1$, $N = 100$, and $f = 0.5$ in part a and $\bar{\phi} = 0.05$, $l_B = 1$, $\chi = 3$, and $f = 0.5$ in part b.

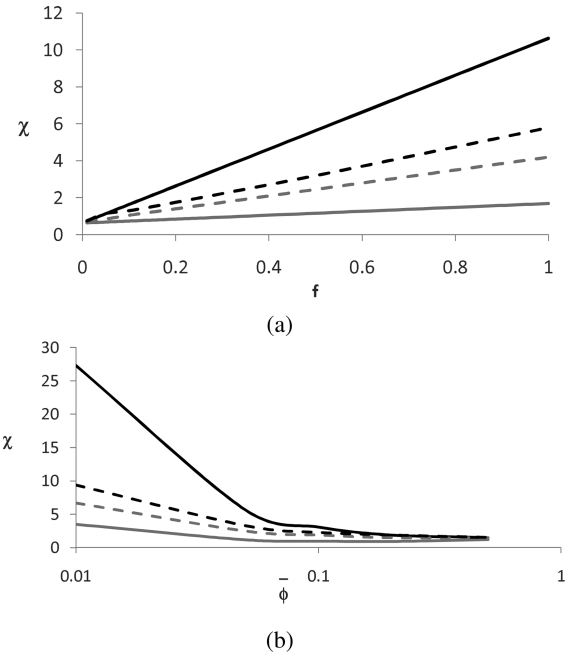

Figure 5. Critical solvent qualities against (a) charge fraction and (b) isotropic volume fraction evaluated by the RPA and nonlinear (NL) analysis. Black and gray lines are predictions for χ_{mi} and χ_{ma}, respectively. Bold and dashed lines are predictions of RPA and NL approaches, respectively. Micro(nano)phase separation is expected to occur between the black and gray lines. The model parameters are $\bar{\phi} = 0.05$, $l_B = 1$, and $N = 100$ in part a and $f = 0.5$, $l_B = 1$, and $N = 100$ in part b.

expected to be first-order in nature. Moreover, given electroneutrality in each cell, the system will shrink in volume by releasing water. We note that the formation of the respective domains consisting of swollen and of collapsed chains gives rise to a complex mechanism of charge regulation, reminiscent of the domains observed in grafted charged chains in poor solvent backbones.[20] In the present work, we do not account for changes in dielectric permittivity (documented in studies of charged gels in a poor solvent[21]), which will generally lead to ion adsorption at liquid interfaces separating dielectric inhomogeneities.[22−25] We also ignore the possibility of forming necklace conformations that have been predicted in solutions of weakly charged chains with hydrophobic backbones[26,27] and observed in networks of hydrophobic chains with charged groups.[28]

In summary, the excess charge−density profiles in the nanophase-separation regime clearly show the presence of dense segregated regions alternated by depleted regions. However, there exists an interfacial energy cost associated with the creation of sharp interfaces between these regions. Because this behavior is not properly accounted for in the conventional linear-response (RPA) approach, the stability region of the nanophase-segregated structure found from the nonlinear numerical solution turns out to be smaller than that found using RPA. Our 1D model should serve as a useful guide to the analysis of the more general 3D problem. First, we are able to obtain approximate analytical expressions describing the onset of various phase-separation regimes. Second, the framework of our 1D formulation can be straightforwardly generalized to the 3D case without additional fundamental changes in our formalism. Aside from the generalization to three dimensions, we can also consider a nonzero salt concentration in our analysis. The presence of salt (and, in particular, multivalent salt) may lead to a plethora of new behaviors because of the effects of screening, ion-pairing, and ion condensation.[29−33] From the modeling perspective, these aforementioned effects have a few qualitative consequences. In particular, salt ions in the reservoir introduce both coions and counterions into the system and thus can permit ion exchange with the reservoir without violating electroneutrality. As such, we can no longer neglect the reservoir contribution to the free energy. The influence of other environmental conditions (e.g., pH, electric field, chemical reactions, etc.) may also be studied along similar lines of reasoning. It will be interesting to include fluctuations in our present Green's function formalism, following the recent field-theoretical approach developed to study the phenomenon of PE complexation.[34]

Acknowledgment. We thank Dr. Graziano Vernizzi and Dr. William Kung for useful discussions. This work was supported by NSF grant DMR-0520513 of the MRSEC program at Northwestern University. P.K.J. acknowledges the MRSEC fellowship for support.

References and Notes

(1) Chaterji, S.; Kwon, K.; Park, K. *Prog. Polym. Sci.* **2007**, *32*, 1083–1122.
(2) Kwon, H. J.; Gong, J. P. *Curr. Opin. Colloid Interface Sci.* **2006**, *11*, 345–350.
(3) Malmsten, M. *Soft Matter* **2006**, *2*, 760–69.
(4) Khademhosseini, A.; Langer, R. *Biomaterials* **2007**, *28*, 5087–92.
(5) Ahn, S.; Kasi, R. M.; Kim, S.; Sharma, N.; Zhou, Y. *Soft Matter* **2008**, *4*, 1151–57.
(6) Mano, J. F. *Adv. Eng. Mater.* **2008**, *10*, 515–527.
(7) Lendlein, A.; Kratz, K.; Kelch, S. *Med. Device Tech.* **2005**, 12–15.
(8) Shibayama, M. *Macromol. Chem. Phys.* **1998**, *199*, 1–30.
(9) Ikkai, F.; Shibayama, M. *Polymer* **2007**, *48*, 2387–2394.
(10) Zeldovich, K. B.; Dormidontova, E. E.; Khokhlov, A. R.; Vilgis, T. A. *J. Phys. II* **1997**, *7*, 627–635.
(11) Onuki, A. *Phase Transitions Dynamics*; Cambridge University Press: Cambridge, U.K., 2002.
(12) Rabin, Y.; Panyukov, S. *Macromolecules* **1997**, *30*, 301–312.
(13) Slater, G. W.; Gratton, Y.; Kenward, M.; McCormick, L.; Tessier, F. *Soft Mater.* **2004**, *2*, 155–182.
(14) de Gennes, P.-G. *Scaling Concepts in Polymer Physics*; Cornell University Press: Ithaca, NY, 1979.
(15) Chaikin, P. M.; Lubensky, T. C. *Principles of Condensed Matter Physics*; Cambridge University Press: Cambridge, U.K., 1995.

(16) Jackson, J. D. *Classical Electrodynamics*; Wiley: New York, 1999.
(17) Marshall, S. L. *J. Phys.: Condens. Matter* **2000**, *12*, 4575–4601.
(18) Avriel, M. *Nonlinear Programming: Analysis and Methods*; Dover Publications, Inc.: New York, 2003.
(19) Luenberger, D. G. *Linear and Nonlinear Programming*; Addison-Wesley: Reading, MA, 1984.
(20) Sandberg, D. J.; Carrillo, J. Y.; Dobrynin, A. V. *Langmuir* **2007**, *23*, 12716–12728.
(21) Schneider, S.; Linse, P. *Macromolecules* **2004**, *37*, 3850–3856.
(22) Dzubiella, J.; Swanson, J. M. J.; McCammon, J. A. *J. Chem. Phys.* **2006**, *124*, 084905.
(23) Dzubiella, J.; Swanson, J. M. J.; McCammon, J. A. *Phys. Rev. Lett.* **2006**, *96*, 087802.
(24) Kung, W.; Solis, F. J.; de la Cruz, M. O. *J. Chem. Phys.* **2009**, *130*, 044502.
(25) Bier, M.; de Graaf, J.; Zwanikken, J.; van Roij, R. *J. Chem. Phys.* **2009**, *130*, 024703.
(26) Dobrynin, A. V.; Rubinstein, M. *Macromolecules* **1996**, *29*, 2974–2979.
(27) Solis, F. J.; de la Cruz, M. O. *Macromolecules* **1998**, *31*, 5502–5506.
(28) Mann, B. A.; Kremer, K.; Holm, C. *Macromol. Symp.* **2006**, *237*, 90–107.
(29) Dobrynin, A. V. *Curr. Opin. Colloid Interface Sci.* **2008**, *13*, 376–388.
(30) de la Cruz, M. O. *Soft Matter* **2008**, *4*, 1735–1739.
(31) Solis, F. J.; Vernon, B. *Macromolecules* **2007**, *40*, 3840–3847.
(32) Edgecombe, S.; Linse, P. *Macromolecules* **2007**, *40*, 3868–3875.
(33) Yin, D. W.; Horkay, F.; Douglas, J. F.; de Pablo, J. J. *J. Chem. Phys.* **2008**, *129*, 154902.
(34) Popov, Y. O.; Lee, J.; Fredrickson, G. H. *J. Polym. Sci., Part B* **2007**, *45*, 3223–3230.